High-Harmonic Gravity Signatures Related to Post-Glacial Rebound

H.H.A. Schotman[1,2], P.N.A.M. Visser[1], L.L.A. Vermeersen[1]

[1] Delft Institute of Earth Observation and Space Systems (DEOS), Faculty of Aerospace Engineering, Delft University of Technology, Kluyverweg 1, 2629 HS Delft, The Netherlands
[2] SRON Netherlands Institute for Space Research, Sorbonnelaan 2, 3584 CA, Utrecht, The Netherlands

Abstract. The earth's shallow layers, up to a depth of about 200 km, can have viscosities that are an order to several orders of magnitude lower than those of surrounding layers. These layers can induce high-harmonic (degree and order 50 - 150) gravity anomalies due to the ice and meltwater redistribution in the last glacial cycle. Uncertainties in ice-load histories will induce gravity and geoid anomaly differences in these high harmonics. The GOCE satellite mission is expected to be able to discern differences between various Late-Pleistocene ice-load histories and is also predicted to be sensitive enough to detect the effects of shallow low-viscosity crustal and asthenosphere zones. For example, our earth relaxation models indicate that GOCE should be sensitive to typical differences between ice-load histories up to harmonic degree 140 for a crustal low-viscosity zone and up to harmonic degree 70 for a low-viscosity zone in the asthenosphere. GRACE is mainly sensitive to differences for the latter. We show that for the limiting case of a lateral homogeneous earth, it is possible to constrain properties of crustal low-viscosity layers in the presence of uncertainties in the ice-load history.

Keywords. low-viscosity earth layers, post-glacial rebound, satellite gravity

1 Introduction

Late-Pleistocene Ice-Age cycles have left observable markings at the earth's surface. Examples include the ongoing post-glacial rebound (PGR) in Fennoscandia and Canada, and secular variations in the earth's rotation. Furthermore, in the geoid and in gravity anomalies the remaining solid-earth deviations from isostasy following the ice and meltwater redistribution from the last glacial cycle are detectable. Magnitudes and spatial patterns of these geoid and gravity anomalies are dependent on two variables: the ice- and water-load distribution history on one side, and material and rheological variables of the solid earth on the other. The earth's shallow layers, up to a depth of about 200 km, can have viscosities that are an order to several orders of magnitude lower than those of surrounding layers. Beneath oceanic areas the asthenosphere, i.e. the uppermost layer of the mantle, can have such low-viscosity zones (LVZs, see e.g. Pollitz (2003), Stein and Wysession (2003, p. 170)), whereas in continents LVZs can exist in the lower crust (see e.g. Watts and Burov (2003); Ranalli and Murphy (1987)). The layers can superimpose high-harmonic (degree and order 50 - 150) contributions (van der Wal et al., 2004) upon the generally low-harmonic (smaller than 50) geoid anomalies resulting from mantle relaxation. Typical amplitudes are a few decimeters underneath and just outside formerly glaciated areas, with scales down to hundred kilometers. Changes in the properties of these crustal LVZs (CLVZs) and asthenospheric LVZs (ALVZs) and uncertainties in the ice-load histories will induce geoid and gravity anomaly differences in these high harmonics with the same order of magnitude and similar resolution.

The GOCE satellite mission, to be launched by ESA in February 2007, is predicted to measure the static gravity field with an accuracy of 1 cm in geoid height and 1 mgal in gravity anomaly at 100 km resolution (Visser et al., 2002). Such accuracy and resolution opens the possibility to discern differences between various Late-Pleistocene ice-load histories and constrain properties of CLVZs and ALVZs. Several studies on the effect of a CLVZ on PGR observables have been performed in the past years, see e.g. Klemann and Wolf (1999); Di Donato et al. (2000); Kendall et al. (2003); Vermeersen (2003). In this paper we concentrate on gravity anomalies induced by CLVZs and ALVZs. We investigate the sensitivity of the response to a CLVZ and an ALVZ by using two different ice-load histories: a modified version of ICE3G (Tushingham and Peltier, 1991), and a more recent model by Kurt Lambeck (see e.g. Lambeck et al. (1998)).
We show using spherical harmonic degree amplitudes, that for a CLVZ the differences are above the expected GOCE error level or *performance* up to spherical harmonic degree 140 and for an ALVZ up to de-

gree 70. This performance estimate is based on formal errors as described in Visser et al. (2002). The differences are also above the realized GRACE performance over a 363-day period (GGM02S, Tapley et al. (2005)); up to degree 90 for a CLVZ and degree 60 for an ALVZ. Note that the GRACE performance will improve if a longer measurement period is used, though this will mainly affect the long-wavelength part. This means that GRACE, but especially GOCE, could provide information on the ice-load history in the presence of an LVZ. If we are however interested in constraining properties of an LVZ, uncertainties in the ice-load history are an error source. We show that even in the presence of uncertainties in the ice-load history, it is possible to extract information on LVZs, using spectral signatures. In future studies, we will concentrate on extracting information on LVZs in the presence of other error sources, as errors in modelling time-variable processes (tides, atmospheric and hydrological mass variations, see Han et al. (2006)), unmodelled crustal and lithospheric mass inhomogeneities due to compositional, thermal and thickness variations, and (shallow) mantle heterogeneities due to for example subduction (Mikhailov et al., 2004) and mantle plumes.

2 Theory

In this section, we will concentrate on the definition of the geoid height and gravity anomaly, and how these are computed from potential coefficients, as delivered by GOCE and GRACE, and in our PGR model.

2.1 Gravity Field from Potential Coefficients

If there are no masses above the geoid, or if these have been properly removed, the *disturbing* potential, i.e. the difference between the actual potential and a *normal* potential in the same point, outside the geoid can in spherical approximation be expanded as (Heiskanen and Moritz, 1967, p. 35):

$$T = \frac{GM}{R} \sum_{n=0}^{N} \left(\frac{R}{r}\right)^{n+1} \sum_{m=0}^{n} \overline{C}_{nm} Y_{nm} \tag{1}$$

where G is Newton's gravitational constant, M and R are the mass and radius of the earth, N is the maximum degree of expansion, r is the distance to the center of the earth, $\overline{C}_{nm}$ are the fully normalized, *dimensionless* potential (or *Stokes*) coefficients of degree n and order m, and Y_{nm} are fully normalized surface spherical harmonics.
The *geoid* is defined as the surface that has the same potential as a reference surface (e.g. the GRS80 ellipsoid). The coefficients of the *geoid height*, the distance between the geoid and the reference surface, can then be computed by using *Brun's formula* (Heiskanen and Moritz, 1967, p. 85), which in our notation reads:

$$N_{nm} = R \cdot \overline{C}_{nm} \tag{2}$$

The *gravity anomaly* is defined as the difference between the gravity acceleration (i.e. the negative of the potential gradient) on the geoid and the normal gravity on the reference surface, and is equal to (Heiskanen and Moritz, 1967, p. 85):

$$\Delta g = -\frac{\partial T}{\partial r} + \frac{1}{\gamma_0}\frac{\partial \gamma}{\partial r} T \tag{3}$$

where $\gamma_0 = GM/R^2$ is the normal gravity at the reference surface. The term $\partial\gamma/\partial r$ can be regarded as the *free-air correction* and is on the surface of the earth equal to:

$$\left(\frac{\partial \gamma}{\partial r}\right)_{r=R} = \left(\frac{\partial GM/r^2}{\partial r}\right)_{r=R} = -2\frac{\gamma_0}{R} \tag{4}$$

This gives for eq. 3 (Heiskanen and Moritz, 1967, p. 89):

$$\Delta g = -\frac{\partial T}{\partial r} - \frac{2}{R} T \tag{5}$$

Putting expansion eq. 1 for T, we find for the coefficients of the gravity anomaly:

$$\Delta g_{nm} = \gamma_0 \cdot (n-1)\overline{C}_{nm} \tag{6}$$

From this equation, gravity anomalies can be computed from a set of dimensionless geopotential coefficients $\overline{C}_{nm}$ as for example provided by GOCE and GRACE.

2.2 Gravity Field Computation in Post-Glacial Rebound

In PGR studies, it is common to compute elastic load Love numbers in the Laplace-transformed domain for an elastic earth. An inverse Laplace transformation then yields *viscoelastic* Love numbers in the time domain (according to the correspondence principle, see e.g. Peltier (1974)). We use a semi-analytical normal-mode relaxation model (Peltier, 1974; Wu and Peltier, 1982; Vermeersen and Sabadini, 1997) to compute the Love numbers in the Laplace domain.
The dimensionless potential *perturbation* coefficients at the *undeformed* surface, which is in this formalism the reference surface, are equal to (Wahr et al., 1998; Johnston and Lambeck, 1999):

$$\overline{C}_{nm} = \frac{3\rho_L}{\rho_E}\frac{1+k_n}{2n+1} * \overline{L}_{nm} \tag{7}$$

where ρ_L and ρ_E are the density of the load and the mean density of the earth respectively, k_n is the viscoelastic load Love number for potential perturbation of degree n, the asterisk denotes convolution in time and $\overline{L}_{nm}$ are the dimensionless, normalized coefficients of the load thickness. Note that the geoid height, which can again be computed using eq. 2, is now derived from the disturbing potential on the reference surface and not on the geoid, under the assumption that the actual gravity acceleration g at the geoid is equal to the normal gravity at the reference surface γ_o.

To compute the gravity anomaly we proceed as in Mitrovica and Peltier (1989). First we compute the gravity perturbation at the deformed surface *under* the surface mass load (Longman, 1963), which consists of three terms (Farrell, 1972):

- the change in acceleration from moving through the perturbed gravity field, proportional to the radial displacement Love number h_n;
- the direct attraction of the mass load (the 1-term in eq. 7);
- effect of mass redistribution, proportional to k_n.

We cannot compute the direct attraction due to the surface mass load using expansion eq. 1, as this is only valid outside the masses. Instead we have to use the expansion (Heiskanen and Moritz, 1967, p. 34):

$$T = \frac{GM}{R} \sum_{n=0}^{N} \left(\frac{r}{R}\right)^n \sum_{m=0}^{n} \overline{C}_{nm} Y_{nm} \tag{8}$$

Using the free-air correction as an approximation for the gravity change in the unperturbed field, and taking the gradient of eq. 8 for the direct part and of eq. 1 for the internal mass distribution part, we find (Longman, 1963):

$$\Delta g^S_{nm} = \gamma_0 \frac{3\rho_L}{\rho_E} \frac{-n + (n+1)k_n - 2h_n}{2n+1} * \overline{L}_{nm} \tag{9}$$

In Mitrovica and Peltier (1989) this is called the gravity anomaly at the perturbed surface. To obtain the gravity anomaly (at the geoid), Mitrovica and Peltier (1989) move eq. 9 to the geoid through the unperturbed field to obtain:

$$\Delta g_{nm} = \gamma_0 \frac{3\rho_L}{\rho_E} \frac{-(n+2) + (n-1)k_n}{2n+1} * \overline{L}_{nm} \tag{10}$$

Note that this result can be obtained directly by using the appropriate expansions for eq. 7 (eq. 8 for the direct term and eq. 1 for the mass redistribution term proportional to k_n) and using eq. 5, showing the consistency of eq. 6 and eq. 10.

Table 1. Viscosity stratification of our earth models

Layer	Depth [km]	Viscosity [Pas] CLVZ	ALVZ
lithosphere	0–20	$1 \cdot 10^{50}$	$1 \cdot 10^{50}$
	20–32	$1 \cdot 10^{18}$	
	32–80	$1 \cdot 10^{50}$	
upper mantle	80–115	$5 \cdot 10^{20}$	$1 \cdot 10^{18}$
	115–400		$5 \cdot 10^{20}$
	400–670	$5 \cdot 10^{20}$	$5 \cdot 10^{20}$
lower mantle	670–2891	$5 \cdot 10^{21}$	$5 \cdot 10^{21}$
core	2891–6371	0	0

3 Input Parameters

3.1 Earth Stratification

The earth model is radially stratified, incompressible, Maxwell viscoelastic and self-gravitating. We choose a model for a crustal low-viscosity zone (CLVZ) with a lower crust starting at a depth of 20 km, with a thickness of 12 km and a viscosity of 10^{18} Pas. The total lithospheric thickness is 80 km. We have modelled an asthenospheric low-viscosity zone (ALVZ) below a fully elastic lithosphere of 80 km, with a thickness of 35 km and a viscosity of 10^{18} Pas. The total viscosity stratification of our models is given in Table 1. We take volume-averaged densities and elastic parameters from the earth model PREM (Dziewonski and Anderson, 1981).

Note that our current model is laterally homogeneous, which is not very realistic, as it can for example be expected that there are no CLVZs in old and cold lithosphere as for example in Scandinavia. In general CLVZs can be expected in parts of the continental crust with relatively high geothermal heat flux, and ALVZs can be expected more globally, especially below oceanic lithosphere, though with variable thickness.

3.2 Ice- and Sea-Load History

We use an ice-load history of Kurt Lambeck and coworkers from ANU, Canberra (see e.g. Lambeck et al. (1998)) as our reference, and a modified version of ICE3G (Tushingham and Peltier, 1991), which we denote I3G, to test the sensitivity of the gravity anomaly perturbations. The modifications to ICE3G are: scaling up of the volume by 20% to an ice-equivalent sea level[1] of about -130 m at last glacial maximum (LGM), filtering to remove holes that arise due to the finite disc definition of ICE3G, and interpolation to

[1] The ice-equivalent sea level is equal to the ice mass at a particular time, converted to ocean volume by the density of sea water, divided by the ocean area at that particular time. It is equal to the eustatic sea level change if all the ice mass at that particular time would melt.

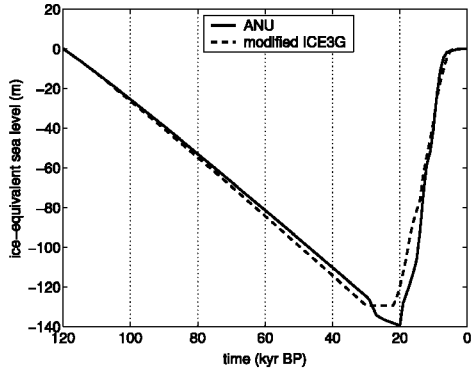

Fig. 1. Ice-equivalent sea level for the ANU and modified ICE3G (I3G) ice-load history

calibrated carbon years, as ICE3G is given in uncalibrated carbon years. We added a phase of constant volume from 30 kyrs BP to LGM ($\approx$ 21 kyr BP) and a linear glaciation phase of 90 kyr starting from 120 kyr BP. The latter is also added to the ANU model, which has an ice-equivalent sea level of 130 - 140 m from 30 kyr BP to LGM. In both models, 99% of the ice melted before 6 kyr BP. In Figure 1 we have plotted the ice-equivalent sea levels for both histories.
In Figure 2 and 3 we have given the ice-load distribution at LGM of the ANU and I3G ice-load histories respectively. The major differences between the models are the larger volume of the Laurentide ice sheet and the smaller (excess) volume over Greenland in the ANU model. The large ice volumes over the Kara Sea and in East-Siberia in the ICE3G model are currently considered to be unrealistic (see e.g. Siegert and Dowdeswell (2004)).
We have included the effect of coastline migration and meltwater influx in areas that were once-glaciated and are now below sea level, as described in Mitrovica and Milne (2003), Lambeck et al. (2003) and Schotman and Vermeersen (2005). We have not considered the effect of rotation and have used only one glacial cycle, as the effect of additional glacial cycles on perturbations is small.

4 Results

As we are interested in gravity anomaly *perturbations* due to an LVZ, we subtract from the results for a model with an LVZ a model without an LVZ. This means that we subtract the results of a model that has the same number of layers as the model with an LVZ, but with a viscosity value for the LVZ that is either very large (i.e. effectively elastic, for a CLVZ) or equal to the upper mantle viscosity (for an ALVZ). Our reference earth model for a CLVZ and an ALVZ is given in Table 1, and our reference ice-model is ANU. To investigate the effect of different properties of the LVZ or different ice-load histories, we use

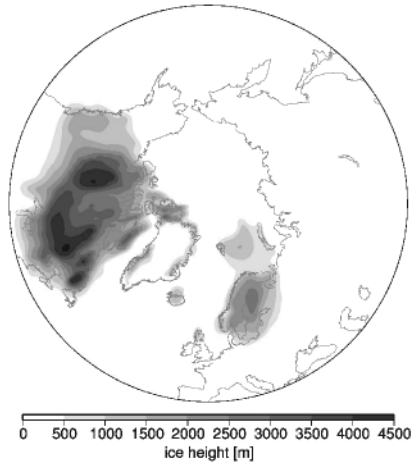

Fig. 2. ANU ice-load distribution at LGM

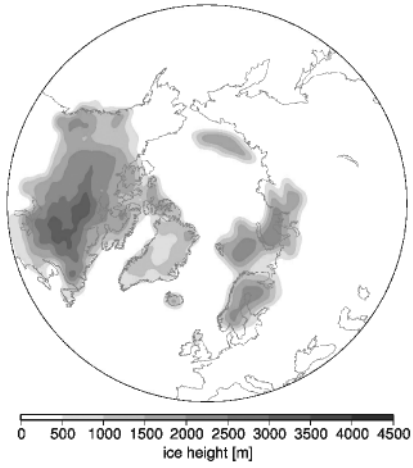

Fig. 3. I3G (modified ICE3G) ice-load distribution at LGM

perturbation *differences*, i.e. the difference between perturbations computed with a certain set of earth- or ice-model parameters and perturbations computed with our reference model.

4.1 PGR- and LVZ-Induced Gravity Anomalies

In Figure 4 we show the predicted gravity anomaly due to PGR, i.e. without an LVZ, using ice-load history ANU. The signal is dominated by negative anomalies in the Hudson Bay area, where mantle material has been pushed towards the bulges, which are the areas with positive anomalies around North-America. The same effect can be seen in Scandinavia.
Next we show gravity anomaly *perturbations* due to a CLVZ, again using ANU (Figure 5). The picture is dominated by small scale perturbations near the edge of the ice-load due to extra mass flow away from glaciated areas during glaciation. As the introduction of a CLVZ increases the relaxation time (Schotman

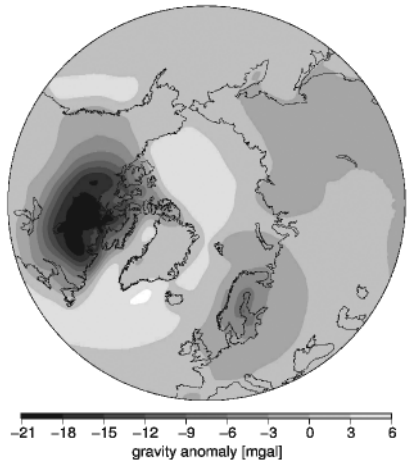

Fig. 4. PGR-induced gravity anomaly (no LVZ)

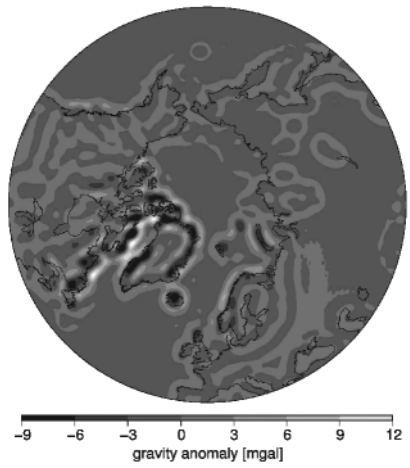

Fig. 5. CLVZ-induced gravity anomaly perturbation

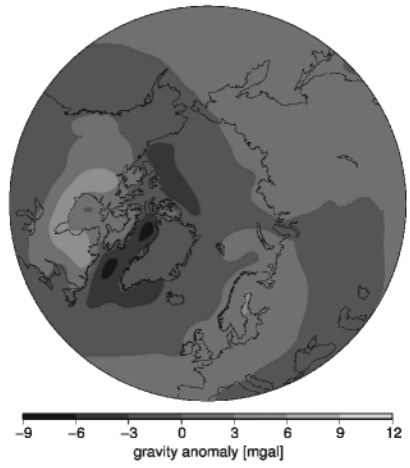

Fig. 6. ALVZ-induced gravity anomaly perturbation

and Vermeersen, 2005) and as the glaciation period is much longer than the deglaciation period, mass has yet to flow back to previously glaciated areas. Perturbation amplitudes are up to 10 mgal which is not small in comparison to the total signal (Figure 4) and the expected performance of GOCE.
Due to the larger depth of the ALVZ, Figure 6 shows less spatial detail than Figure 5. Moreover, because an ALVZ shortens the relaxation time (Schotman and Vermeersen, 2005), adjustment to isostasy is faster, leading to negative perturbations in the bulge areas and positive perturbations in formerly glaciated areas.

4.2 Comparison with the Performance of GOCE and GRACE

To compare the computed gravity anomaly perturbations with GOCE we use degree amplitudes. These are the square roots of the spherical harmonic expansion degree variances of the perturbed field. For gravity anomaly perturbations the degree amplitudes are (compare eq. 6):

$$a_n = \gamma_0 \cdot (n-1)\sqrt{\sum_{m=0}^{n} \overline{C}_{nm}\overline{C}^{*}_{nm}} \qquad (11)$$

where the asterisk denotes complex conjungation.
In Figure 7 we have plotted the CLVZ- and ALVZ-induced perturbation degree amplitudes, the expected performance of GOCE and the realized performance of GRACE (GGM02S). The CLVZ-induced gravity anomaly perturbations are above the GOCE performance up to harmonic degree 140 and above GGM02S up to degree 90. The ALVZ-induced gravity anomaly perturbations have significant amplitude for low degrees; in particular, they are above the GOCE performance up to degree 70 and above GGM02S up to degree 60. This means that GOCE compared to GRACE will probably not add much information on ALVZs, though the ratio of signal to error is more favorable for GOCE, so GOCE is especially predicted to deliver more information on CLVZs.
In following, we will concentrate on CLVZs only. One of the largest uncertainties in PGR modeling is the ice-load history. From Figure 8, where we have plotted perturbation *differences*, we see that GOCE is sensitive to uncertainties in the ice-load history ('I3G-ANU'); as the difference in perturbations between a model using I3G and our reference model (using ANU) is above the performance of GOCE up to degree 140. In Figure 8 we have plotted the differences between a model with either a thicker CLVZ ('t20-t12') or higher viscosity CLVZ ('v19-v18') than our reference model. We see that GOCE is predicted to be sensitive to changes in the properties of the CLVZ up to degree 120-140. Moreover, we see that the curves

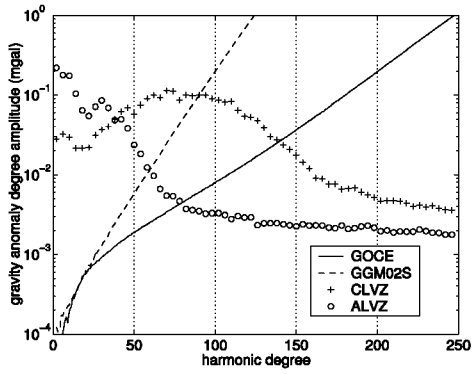

Fig. 7. CLVZ and ALVZ induced perturbations in gravity anomaly degree amplitudes, compared with the performance of GOCE and GGM02S

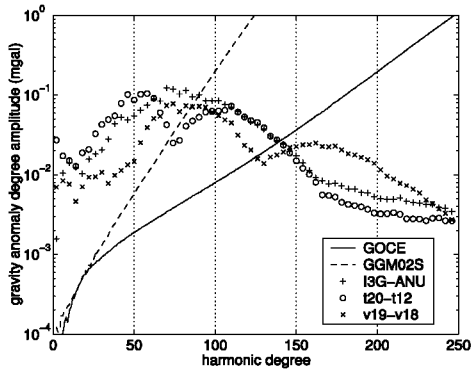

Fig. 8. Differences in CLVZ induced perturbations in gravity anomaly degree amplitudes due to different properties of the CLVZ and different ice-load histories, compared with the performance of GOCE and GGM02S

have a specific form, which is related to the different behavior for a thicker CLVZ and a higher viscosity CLVZ. Further on we will deduce from these curves spectral signatures for different properties of the CLVZ.

From Figure 8 we conclude that in principle GOCE data will add constraints to estimates of the ice-load history in the presence of a CLVZ (with known parameters) and about properties of a CLVZ (if the ice-load history is known). In practice, things are more complicated, because the measured gravity signal consists of large number of contributions, see Section 1. If we consider the gravity field as given by GGM02S, in the spectral range where we expect the largest amplitude (from degree 40 to 90, compare Figure 9), we see no direct relation with the modeled gravity anomalies induced by a CLVZ (Figure 5). Short-scale features are visible, but the amplitudes are much larger than predicted by our PGR model. This means that we have to remove other geophysical signals from the measured gravity field. If models for these geophysical signals are available, the question is if the information on CLVZs is still recoverable in the presence of errors in these models (compare Velicogna and Wahr (2002)).

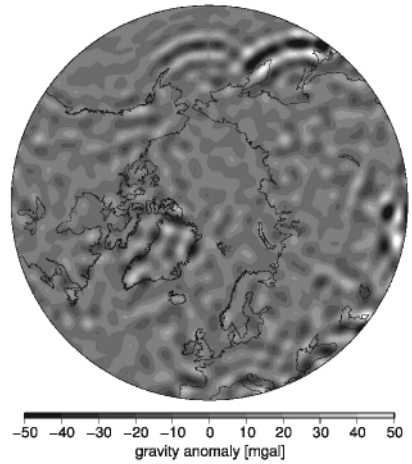

Fig. 9. GGM02S gravity anomalies from harmonic degree 40 to 90

If we assume that all other processes have been removed error-free, then the only uncertainty in this hypothetical case is the ice-load history. In the next section we will show that it is still possible to extract information on the properties of CLVZs from GOCE data in the presence of uncertainties in the ice-load history.

4.3 Spectral Signatures

If we regard the differences between the ANU and I3G ice-load histories as realistic uncertainties in the ice-load history, then it is already clear from Figure 9 that it will be difficult to extract information from GOCE data on the properties of the CLVZ. This can be illustrated more clearly using the degree correlation coefficient, defined as (Mitrovica and Peltier, 1989):

$$\rho_n = \frac{\sum_{m=0}^{n} \overline{C}_{nm}\overline{D}_{nm}}{\sqrt{\sum_{m=0}^{n} \overline{C}_{nm}\overline{C}^{*}_{nm} \sum_{m=0}^{n} \overline{D}_{nm}\overline{D}^{*}_{nm}}} \qquad (12)$$

with $\overline{C}_{nm}$, $\overline{D}_{nm}$ different sets of spherical harmonic coefficients.

In Figure 10 we have plotted the degree correlation coefficient between gravity anomaly values computed with our reference model (CLVZ from Table 1 and ice-model ANU) and different test model values. If our test model is the same as our standard model, then the degree correlation coefficient will be equal to one (not plotted). If we use in our test model the I3G ice-load history, then the correlation between the reference and test model is very poor ($\rho(\Delta g_{ANU}, \Delta g_{I3G})$). If we know the ice-load history, then we can clearly distinguish between a model with a thicker CLVZ

($\rho(\Delta g_{t12}, \Delta g_{t20})$, from degree 70) or a higher viscosity CLVZ ($\rho(\Delta g_{v18}, \Delta g_{v19})$, from degree 100). If we do not know the ice-load history, and correlate for example our reference model with a test model with different parameters of the CLVZ and the I3G ice-load history, then the degree correlation coefficient will be poor due to the bad correlation for different ice-load histories (not plotted), and we cannot constrain the properties of the CVLZ.

This means that we cannot extract information on the properties of the CLVZ in the presence of uncertainties in the ice-load history. A large part of this uncertainty can be removed by normalizing the degree amplitudes with the degree amplitudes of the ice-load history at LGM. This is because the computed free-air gravity anomaly perturbations are a convolution of the temporal and spatial impulse response of the earth (i.e. the time-dependent Love numbers for a certain CLVZ) and the time- and space-dependent input sequence (i.e. the ice-load history). If we consider the response at a certain time interval and assume the ice-load is constant (which is obviously not the case), then the spatial spectrum (i.e. the degree amplitudes) of the impulse response is equal to the ratio of the spectrum of the output (i.e. the gravity anomalies) and the ice-load. The assumption of constant ice load is approximated by using the ice load at LGM, which is justified by the long period of glaciation compared to deglaciation. In Schotman and Vermeersen (2005) we have shown that the computed normalized degree amplitudes closely resemble the time-dependent Love numbers for a certain CLVZ as a function of harmonic degree.

In practice, we do not know the real ice-load history, but we can estimate which ice-load history best fits the gravity anomaly perturbations by correlating the spatial spectrum of the gravity anomaly perturbations with the spectrum of the ice-load history (at LGM). We see from Figure 11 that the correlation is always significantly better for the ice model that generated the anomaly perturbations. Moreover we see that the ANU ice model correlates up to higher degree with the corresponding gravity anomalies than the I3G ice model, mainly because the I3G model has less power in the high harmonics.

In Figure 12 we show perturbation degree amplitudes computed with I3G and ANU, normalized by the dimensionless degree amplitudes of the I3G and ANU ice height at LGM, respectively. We can see that the curves are very close, except above degree 70, where the correlation of the perturbations computed from I3G and the ice heights of I3G drop very fast, see Figure 11. If we consider the degree correlations from Figure 11 as a measure for the quality of the normalized degree amplitudes, we can compute a best estimate from the two normalized degree amplitude curves in a weighted least squares (WLSQ) sense, with weights determined by the degree correlations.

If we follow the same procedure for different properties of the CLVZ we obtain spectral signatures, as plotted in Figure 13. We have plotted only those parts that are above the propagated error, which we have defined as the difference between the normalized degree amplitudes computed using I3G and using ANU (Figure 12), divided by 2. The spectral signature shows that a thicker layer merely moves the maximum to lower degree, whereas a higher viscosity CLVZ shows no change up to degree 50, then deviates from the reference model, and has a maximum for higher degree. Moreover, we have shown that it is possible to obtain information on CLVZs in the presence of uncertainties in the ice-load history, by forward modelling the effect of a CLVZ on gravity anomalies and manipulating the resulting perturbations in the spectral domain.

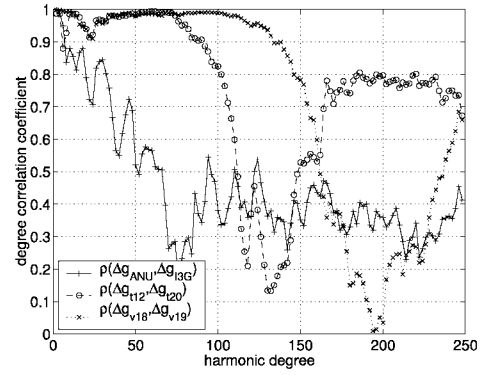

Fig. 10. Degree correlation coefficients between gravity anomaly perturbations computed from reference model and different test models

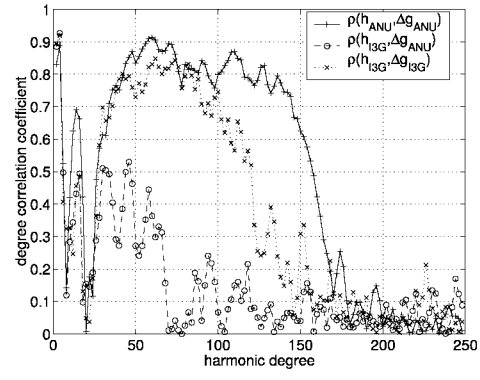

Fig. 11. Degree correlation coefficient between the ANU and I3G ice heigts at LGM, and gravity anomalies computed using the ANU and I3G model

5 Summary and Outlook

We have shown that gravity anomaly perturbations induced by crustal low-viscosity zones (CLVZs) are above the expected GOCE performance up to harmonic degree 140 and above the realized GRACE

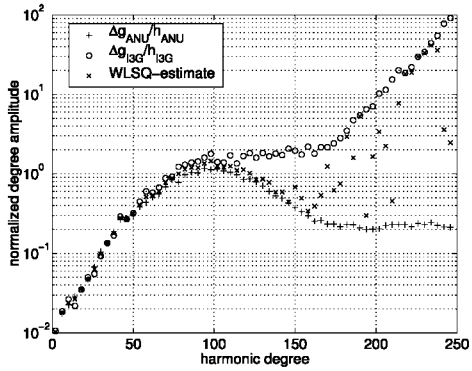

Fig. 12. Spectrum of gravity anomalies scaled with ice heights from ANU, I3G and a weighted least squares estimate

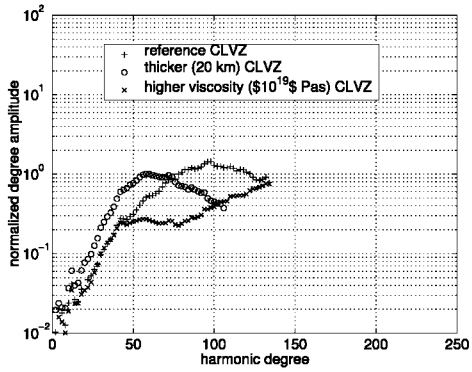

Fig. 13. Spectral signature for different properties of the CLVZ

performance (GGM02S) up to degree 90. For an asthenospheric LVZ (ALVZ) the gravity anomaly perturbations are above the expected GOCE performance and GGM02S up to degree 70 and 60, respectively. GOCE is thus especially useful for detecting CLVZs. It was found that GOCE is also sensitive to changes in rheological properties of a CLVZ, which means that in principle GOCE should be able to constrain the rheology. GOCE is however also sensitive to uncertainties in the ice-load history, though a large part of this uncertainty can be removed by manipulating the data in the spectral domain to obtain spectral signatures for different CLVZs. Note that this study is valid for the limiting case of a laterally homogeneous earth, which is clearly not realistic everywhere with regard to the presence and properties of CLVZs.

In practice, it will be difficult to extract information from satellite gravity data. From a filtered version of GGM02S we have seen that a large number of geophysical signals is present in the gravity field. We therefore need to remove as well as possible all geophysical signals in the frequency range that we are interested in, and use some form of spatio-spectral filtering to isolate the relevant signal (see e.g. Simons and Hager (1997)). In future studies, we will show if this is possible from simulated data with realistic error sources, and GRACE data. For the latter we will use a laterally heterogeneous model (based on finite elements, see e.g. Wu et al. (2005)) and realistic viscosity values computed from seismic data.

6 Acknowledgements

We thank Jerry Mitrovica, an anonymous reviewer and Mark Drinkwater for their constructive comments, Kurt Lambeck and co-workers (ANU, Canberra) for their global ice sheet model and Radboud Koop (SRON, Utrecht) for discussions.

References

Di Donato, G., J.X. Mitrovica, R. Sabadini, and L.L.A. Vermeersen (2000). The influence of a ductile crustal zone on glacial isostatic adjustment; geodetic observables along the U.S. East Coast, *Geophys. Res. Lett.*, 27, pp. 3017–3020.

Dziewonski, A.M. and D.L. Anderson (1981). Preliminary Reference Earth Model, *Phys. Earth Planet. Inter.*, 25, pp. 297–356.

Farrell, W.E. (1972). Deformation of the earth by surface loads, *Rev. Geophys. Space Phys.*, 10, pp. 761–797.

Han, S.-C., C.K. Shum, P. Ditmar, P. Visser, C. van Beelen and E.J.O. Schrama (2006) Aliasing effect of high frequency mass variations on GOCE recovery of the earth's gravity field, *J. Geodyn.*, 41, pp. 69–76.

Heiskanen, W. and H. Moritz (1967). *Physical Geodesy*, W.H. Freeman and Co., San Francisco, 364 pp.

Johnston, P. and K. Lambeck (1999). Postglacial rebound and sea level contributions to changes in the geoid and the earth's rotation axis, *Geophys. J. Int.*, 136, pp. 537–558.

Kendall, R., J.X. Mitrovica and R. Sabadini (2003). Lithospheric thickness inferred from Australian post-glacial sea-level change: The influence of a ductile crustal zone, *Geophys. Res. Lett.*, 30, pp. 1461–1464.

Klemann, V. and D. Wolf (1999). Implications of a ductile crustal layer for the deformation caused by the Fennoscandian ice sheet, *Geophys. J. Int.*, 139, pp. 216–226.

Lambeck, K., C. Smither and P. Johnston (1998). Sea-level change, glacial rebound and mantle viscosity of northern Europe, *Geophys. J. Int.*, 134, pp. 102–144.

Lambeck, K., A. Purcell, P. Johnston, M. Nakada, Y. Yokoyama (2003). Water-load definition in the glacio-hydro-isostatic sea-level equation, *Quat. Sci. Rev.*, 22, p. 309–318.

Longman, I.M. (1963). A Green's function for determining the deformation of the earth under surface mass loads, 2. Computations and numerical results, *J. Geophys. Res.*, 68, pp. 485–496.

Mikhailov, V., S. Tikhotsky, M. Diament, I. Panet, V. Ballu (2004). Can tectonic processes be recovered from new gravity satellite data?, *Earth Planet. Sci. Lett.*, 228, 10.1016/j.epsl.2004.09.035.

Mitrovica, J.X. and G.A. Milne (2003). On post-glacial sea level: I. General theory, *Geophys. J. Int.*, 154, pp. 253–267.

Mitrovica, J.X. and W.R. Peltier (1989). Pleistocene deglaciation and the global gravity field, *J. Geophys. Res.*, 94, pp. 13,651–13,671.

Peltier, W.R. (1974). The impulse response of a Maxwell earth, *Rev. Geophys. Space Phys.*, 12, pp. 649–669.

Pollitz, F.F. (2003). Transient rheology of the uppermost mantle beneath the Mojave Desert, California, *Earth Planet. Sci. Lett.*, 215, pp. 89–104.

Ranalli, G. and D. Murphy (1987). Rheological stratification of the lithosphere, *Tectonophys.*, 132, pp. 281–295.

Schotman, H.H.A. and L.L.A. Vermeersen (2005). Sensitivity of glacial isostatic adjustment models with shallow low-viscosity earth layers to the ice-load history in relation to the performance of GOCE and GRACE, *Earth Planet. Sci. Lett.*, 236, 10.1016/j.epsl.2005.04.008.

Siegert, M.J. and J.A. Dowdeswell (2004). Numerical reconstructions of the Eurasian Ice Sheet and climate during the Late Weichselian, *Quat. Sci. Rev.*, 23, pp. 1273–1283.

Simons, M. and B.H. Hager (1997). Localization of the gravity field and the signature of glacial rebound, *Nature*, 390, pp. 500–504.

Stein, S. and M. Wysession (2003). *Introduction to Seismology, Earthquakes, and Earth Structure*, Blackwell Publishing, Oxford, 498 pp.

Tapley, B., J. Ries, S. Bettadpur, D. Chambers, M. Cheng, F. Condi, B. Gunter, Z. Kang, P. Nagel, R. Pastor, T. Pekker, S. Poole and F. Wang (2005). GGM02 - An improved earth gravity field model from GRACE, *J. Geodesy*, 10.1007/s00190-005-0480-z.

Tushingham, A.M. and W.R. Peltier (1991). ICE3G: A new global model of late Pleistocene deglaciation based upon geophysical predications of postglacial relative sea level change, *J. Geophys. Res.*, 96, pp. 4497–4523.

van der Wal, W., H.H.A. Schotman and L.L.A. Vermeersen (2004). Geoid heights due to a crustal low viscosity zone in glacial isostatic adjustment modeling; a sensitivity analysis for GOCE, *Geophys. Res. Lett.*, 31, 10.1029/2003GL019139.

Velicogna, I. and J. Wahr (2002). Postglacial rebound and earth's viscosity structure from GRACE, *J. Geophys. Res.*, 107, 10.1029/2001JB001735.

Vermeersen, L.L.A. (2003). The potential of GOCE in constraining the structure of the crust and lithosphere from post-glacial rebound, *Space Sci. Rev.*, 108, pp. 105–113.

Vermeersen, L.L.A. and R. Sabadini (1997). A new class of stratified visco-elastic models by analytical techniques, *Geophys. J. Int.*, 139, pp. 530–571.

Visser, P.N.A.M., R. Rummel, G. Balmino, H. Sünkel, J. Johannessen, M. Aguirre, P.L. Woodworth, C. Le Provost, C.C. Tscherning and R. Sabadini (2002). The European earth explorer mission GOCE: Impact for the geosciences, In: *Ice Sheets, Sea Level and the Dynamic Earth*, J.X. Mitrovica and L.L.A. Vermeersen (eds), *AGU Geodynamics Series*, 29, AGU, Washington DC, pp. 95–107.

Wahr, J., M. Molenaar and F. Bryan (1998). Time variability of the earth's gravity field: Hydrological and oceanic effects and their possible detection using GRACE, *J. Geophys. Res.*, 103, pp. 30,205–30,229.

Watts, A.B. and E.B. Burov (2003). Lithospheric strength and its relationship to the elastic and seismogenic layer thickness, *Earth Planet. Sci. Lett.*, 213, pp. 113–131.

Wu, P. and W.R. Peltier (1982). Viscous gravitational relaxation, *Geophys. J. R. Astron. Soc.*, 70, pp. 435–485.

Wu, P., H. Wang and H. Schotman (2005) Postglacial induced surface motions, sea-levels and geoid rates on a spherical, self-gravitating, laterally heterogeneous earth, *J. Geodyn.*, 39, pp. 127–142.